https://doi.org/10.5194/egusphere-2025-5633
Preprint. Discussion started: 5 December 2025

Seasonal dynamics of vegetation effect on peatland surface energy balance

Vincent E. Flemming[1], Nicolas Behrens[1], Mana Gharun[1]

[1]Institute of Landscape Ecology, University of Münster, Münster, D-48149, Germany

Correspondence to: Vincent E. Flemming (vincent.flemming@uni-muenster.de)

Abstract. Peatland ecosystems play a major role in regulating the climate by storing carbon and modulating surface energy fluxes. While energy fluxes in these ecosystems are strongly influenced by climate conditions, separating the influence of climate and vegetation remains challenging. Here, we analyse eddy covariance measurements collected in 2023 at a degraded raised bog in northwest Germany. Using high-frequency gas flux and meteorological observation data we (1) characterize the annual and seasonal dynamics of radiative and turbulent energy fluxes, (2) quantify the climatic and biotic (i.e., stomatal regulation) controls on latent heat flux (LE), and (3) identify the periods d when vegetation becomes a weaker driver of LE due to stomatal regulation.

To assess the biotic controls on latent heat flux (LE), we examined the role of canopy stomatal conductance and vegetation gross primary productivity (GPP). Canopy conductance (gc) was estimated using the inverted Penman–Monteith equation, which allowed us to model a continuous time series of gc. Abiotic drivers of energy fluxes were evaluated by analysing daily and seasonal patterns of radiation, air temperature, vapor pressure deficit (VPD), and water table depth (WTD). The relative effect sizes of biotic and abiotic drivers were quantified using generalized least squares with autoregressive errors (GLSAR). Our results show that mean daily LE peaks ranged from 8.5 to 215 W m^{-2} in 2023, with seasonal variations in vegetation productivity exerting a strong influence. GPP, VPD, and net radiation emerged as the dominant drivers of LE dynamics, while no relationship with WTD was observed. These findings highlight that both GPP and VPD must be jointly considered in analyses of turbulent energy fluxes, as their interactions exert nonlinear effects on ecosystem–atmosphere exchange of energy.

1 Introduction

Although peatlands cover only 3% of global land area, they store around 30% of global terrestrial soil organic carbon (SOC) (Yu, 2012). Their high water-holding capacity also makes them key regulators of hydrology, buffering both water availability (Karimi et al., 2024) and the impact of droughts (Kettridge and Waddington, 2014). In their natural state peatlands are (nearly) waterlogged ecosystems that naturally sequester and store carbon for centuries. Anthropogenic drainage for agriculture, peat cutting and forestry as well as climate change effects lead to lowered water tables, degradation of the peat and emission of the carbon as CO_2. Intact peatlands possess hydrological self-regulation mechanisms that mitigate drought effects (Nijp et al., 2017), but these capacities are impaired when water levels decline. Lowered water

https://doi.org/10.5194/egusphere-2025-5633
Preprint. Discussion started: 5 December 2025

tables reduce the water-holding capacity of the porous peat matrix, enhancing lateral water loss and altering vertical water vapor fluxes from evaporation (E) and transpiration (T) (Liu et al., 2022). Vegetation change further amplifies these dynamics. In degraded peatlands, increased abundance of species such as Betula spp. can elevate transpiration rates, intensifying vertical water losses (Fay and Lavoie, 2009). Such vegetation shifts are facilitated by both lowered water levels and warming trends (Heijmans et al., 2013) which are expected to intensify under climate change (Shekhar et al., 2024). Understanding the mechanisms that control vertical water vapor transport is therefore critical for effective peatland management and preservation. Ecosystem-scale measurements of water vapor fluxes at high temporal resolution are best obtained using the eddy covariance (EC) method, which directly captures gas exchange between ecosystems and the atmosphere.

While a large body of research focuses on energy fluxes in boreal and tropical peatlands, Central European peatlands remain largely unexplored (Gerling et al., 2019). Water table depth (WTD) has often been examined as a potential control on LE, but most cases report little to no influence (e.g., Gerling et al., 2019; Humphreys et al., 2006). Exceptions occur under extreme conditions: at very low WTD, modest effects on LE have been observed (Gunawardhana et al., 2021; Lafleur et al., 2005), whereas short-term increases in LE have been detected when WTD rises above the soil surface (Liu et al., 2022; Moore et al., 2013). Other factors frequently linked to LE dynamics include net radiation (R_n), vapor pressure deficit (VPD) and air temperature (T_a). Among these R_n emerged consistently as a dominant driver across boreal and alpine peatland ecosystems (e.g., Alekseychik et al., 2017 (raised bog, boreal); Gunawardhana et al., 2021 (alpine sphag. valley bog); Sonnentag et al., 2010 (minerotrophic fen, boreal)). Vegetation composition and functional type also play a critical role, with plant communities exerting stronger influence on LE than peatland type itself (Humphreys et al., 2006).

Against this background, we address the following questions: (i) How does the partitioning of energy fluxes vary seasonally? (ii) What environmental factors most strongly influence the evaporative cooling potential of the peatland ecosystem? (iii) How does vegetation physiological functioning (stomatal regulation) affect energy flux partitioning? We hypothesized that (a) LE exceeds sensible heat flux (H) in summer, while the opposite holds in winter, due to higher VPD and active vegetation during the growing season; (b) R_n is the primary driver of LE, as global radiation (R_g) is the main energy source for the ecosystem; (c) canopy conductance (g_c) – and its influence on LE – is greatest in spring, when leaves are fully developed but stomatal regulation is still weak under low VPD conditions. We used one full year of eddy covariance and micrometeorological measurements from a drained peatland ecosystem in northwest Germany to test these hypotheses.

2 Methods & site description

2.1 Study site

The study area is located in Amtsvenn-Hündfelder Moor (DE-Amv), North Rhine-Westphalia - Germany. This peatland covers an area of 894 ha (Europäische Union, 2021) and has been part of the Natura 2000 network since 2004, which is the world's largest contiguous network of protected areas (Directorate-General for Environment, 2024). Degraded raised bogs

https://doi.org/10.5194/egusphere-2025-5633
Preprint. Discussion started: 5 December 2025

that are still capable of restoration dominate the ecotone, which are characterized by *Calluna vulgaris* (L.) Hull, *Erica tetralix* L. and *Molinia caerulea* (L.) Moench. Species such as *Somatochlora arctica* Zetterstedt or *Drosera intermedia* Hayne occur here and make the area a valuable habitat (Utikal and Rückriem, 2019). According to the Köppen-Geiger climate classification, DE-Amv belongs to type Cfb (warm temperate, fully humid zone with warm summers) (Kottek et al., 2006). Long-term weather data comes from the nearest weather station of the German weather service [ger: Deutscher Wetterdienst] (DWD) in Ahaus (52°04'52.7 "N 6°56'27.2 "E, ID: 7374) (DWD, 2022): The average annual temperature between 2007 and 2024 was 10.6 °C, with the coldest month being January with an average temperature of 1.1 °C and the warmest month being July with 18.3 °C. The mean annual precipitation is 794 mm (2007 – 2024). Maintenance measures within DE-Amv are mainly grazing and de-thatching, which are carried out to preserve and enhance the protected area (Utikal and Rückriem, 2019). DE-Amv is currently in the process of rewetting. An eddy tower is located at 52°10'33.6 "N 6°57'18.0 "E and has been providing continuous data since October 2022. The tower is located at a height of 38 m above sea level and the eddy covariance setup 2.8 m above the surface. DE-Amv is an official ICOS associate station.

2.2 Data

The eddy covariance data was processed according to standard procedures, including filtering for low u^* conditions and spike removal (Pastorello et al., 2020). A detailed list of all available variables and measuring devices used can be found in Table 1. Missing data in meteorological variables was filled from a small meteorological ancillary tower, located 20 m from the EC tower. Additional remaining gaps were filled with XGBoost (Chen and Guestrin, 2016). Results of the gap-filling were verified on test datasets left out during model training and R^2 scores exceeded 0.85 for all gaps. The own data processing was done with Python 3 (van Rossum and Drake, 2009), in particular the packages Numpy (Harris et al., 2020), Pandas (The pandas development team, 2025), SciPy (Virtanen et al., 2020), scikit-learn (Pedregosa et al., 2011), statsmodels (Seabold and Perktold), Ruptures (Truong et al., 2020), Matplotlib (Hunter, 2007) and Plotly (Plotly Technologies Inc., 2015) were used to perform statistics, mathematics and data handling and to create figures. In this work, EC measurements collected between 2023-01-01 and 2023-12-31 were used. Partitioning of CO2 fluxes into GPP and ecosystem respiration (Reco) was done using the REddyProc package in R (Wutzler et al., 2018).

Table 1: Included variables, measuring devices used and unit of the variables.

Variable	Device	Unit
H_2O	LI7200RS gas analyzer	µmol s^{-1} m^{-2}
wind speed, wind direction	Gill HS50 sonic anemometer	m s^{-1}, °
T_a	Vaisala HMP155	°C
relative humidity (rH)	Vaisala HMP155	%

https://doi.org/10.5194/egusphere-2025-5633
Preprint. Discussion started: 5 December 2025

radiation (R)	Kipp&Zonen CNR4	W m^{-2}
PAR	LI-190R	µmol s^{-1} m^{-2}
(–5 cm) soil temperature (T_s)	Soil T. Thermistor 7900-180	°C
(–5 cm) soil heat flux (SHF)	Hukseflux HFP10SC	W m^{-2}
(–5 cm) soil water content (SWC)	Stevens Hydraprobe	m^3 m^{-3}
Precipitation (P)	TR-525M	mm
Water Table Depth (WTD)	RXMOD-W1	cm

2.3 Energy balance

To evaluate the quality of the eddy covariance measurements, we evaluated the surface energy balance for the study site. Energy balance closure was calculated using the following equation, excluding the effects of snow:

$$E = R_n - SHF - LE - H \, . \quad (1)$$

E represents the error that consists of missing parameters and measurement errors. The sign convention here is that SHF, LE and H are positive upwards, and R_n is positive downwards. To account for the effects of heat storage, data was aggregated to daily values.

2.4 Time series of canopy conductance

Canopy conductance (g_c) was modeled in a modified way according to (Runkle et al., 2014). g_c was first calculated by inverting the Penman-Monteith equation ($g_{c,PM}$), for days where no precipitation (P) on this day and less than 2 mm precipitation the day before occurred (D = {I | P(i)=0 mm P(i-1) < 2 mm}, where D is the set of days used and i is the index of the days) (Dingman, 2015):

$$g_{c,PM} = \frac{g_{at}}{\left(\frac{\Delta \cdot R_n + \rho_a \cdot c_a \cdot g_{at} \cdot e_a^* (1-rH)}{ET \cdot \rho_w \cdot \lambda_v}\right)/\gamma - 1} \, , \quad (2)$$

with gat [m s-1] as atmospheric conductance, λv [MJ kg^{-1}] is the latent heat of vaporization, γ [kPa K^{-1}] is called the psychrometric constant, although it is not a constant, c_a [MJ kg^{-1} K^{-1}] is the heat capacity for air, Δ [kPa K^{-1}] is the slope of relation between saturation vapor pressure (VP) and T_a, e_a^* [kPa] is the saturation VP, ρ_a [kg m^{-3}] is air density and ρ_w [kg m^{-3}] is water density, and c_a [MJ kg^{-1}] is the heat capacity of air. These values were calculated using the following equations:

$$g_{at} \equiv \frac{v_a}{6.25 \ln\left(\frac{z_{veg}+2-0.7z_{veg}}{0.1z_{veg}}\right)} \, , \quad (2a)$$

$$\lambda_v = 2.5 - 2.36 \cdot 10^{-3} \cdot T_a \, , \quad (2b)$$

https://doi.org/10.5194/egusphere-2025-5633
Preprint. Discussion started: 5 December 2025

$$\gamma \equiv \frac{c_a \cdot p_a}{\lambda_v \cdot 0.622}\,, \tag{2c}$$

$$c_a = 1.005 \cdot 10^{-3} + 1.82 \cdot 10^{-3} \cdot \frac{1801.6}{8314.3} \cdot \frac{rH \cdot 6.1078 \cdot 10^{m \cdot T_a/m+T_a}}{T_a+273.15}$$

$$\begin{cases} \forall T_a \geq 0,\ m = 7.5,\ n = 237.4 \\ \forall T_a < 0,\ m = 7.6,\ n = 240.7 \end{cases}, \tag{2d}$$

$$\Delta \equiv \frac{2508.3}{(T_a+237.3)^2} \cdot \exp.^{\frac{17.3 \cdot T_a}{T_a+237.3}}\,, \tag{2e}$$

$$e_a^* = 0.611 \cdot \exp.^{\frac{x \cdot T_a}{T_a+y}}$$

$$\begin{cases} \forall T_a \geq 0,\ x = 17.27,\ y = 237.3 \\ \forall T_a < 0,\ x = 21.87,\ y = 265.5 \end{cases}, \tag{2f}$$

$$\rho_a = \frac{10^3 (p_a - e_a^* \cdot rH)}{287.058(T_a+273.15)} + \frac{10^3 \cdot e_a^* \cdot rH}{461.495(T_a+273.15)}\,, \tag{2g}$$

$$\rho_w = 1000\,. \tag{2h}$$

z_{veg} [m] stands for the vegetation height while m and n are constants, and exp. refers to Euler's number.

It is assumed in the Penman-Monteith method that no energy is advected by water, that evaporation is controlled by the stomata and that no heat storage effects occur. While the heat storage effects can be neglected due to the daily data, precipitation can lead to a violation of the other assumptions. Precipitation leads to interception, which can absorb a relevant part of the energy and due to the evaporation of the interception water the assumption of stomata as the main controlling factor of ET is violated. For this reason, $g_{c,PM}$ was limited to periods without precipitation as mentioned above. To still obtain a continuous time series, the next step was to model gc for all days using the $g_{c,PM}$ data.

To model g_c from the calculated values for all days $g_{c,modeled}$, the following equation from Runkle et al. (2014) was used:

$$g_{c,modeled} \equiv \frac{a \cdot R_g + b}{1 + c \cdot VPD}\,. \tag{3}$$

a, b and c are the best fit variables, R_g and VPD the data in a daily resolution. While Runkle et al. (2014) modeled monthly gc values with equation 3, this approach aimed to achieve a daily resolution. For this purpose of a daily resolution, a moving window of ±15 days was used and $g_{c,PM}$ values in this window were extracted from D and had a selected minimum of four data points. The constants a, b, and c of equation 3 were then adjusted using the curve_fit function of SciPy (Virtanen et al., 2020). The function uses the Levenberg-Marquardt algorithm (Moré, 1977), which is based on the non-linear least squares method. As a quality measure for the model fitting, the root mean square error (RMSE) was used. gc,modeled data was then filtered for the growing season (15th of March to 15th of October). To determine the point at which the evaporative cooling capacity of the vegetation is limited by VPD, gc,modeled and VPD were scattered against each other. If gc,modeled decreases with increasing VPD, gc is limited by VPD.

https://doi.org/10.5194/egusphere-2025-5633
Preprint. Discussion started: 5 December 2025

2.5 Seasonal energy flux dynamics

The annual and daily variations of the energy components (R_n, SHF, H, LE) and other environmental variables (e.g., GPP, T_a) were examined visually. The composition of the turbulent energy fluxes was determined by the Bowen ratio (B). B is given as the ratio of H to LE ($B = H/LE$). To reduce the influence of outliers from negative energy fluxes, particularly during winter, the data was aggregated into three-day values. B was calculated for time periods in which R_g is above 20 W m^{-2}.

2.6 Statistical analysis

Generalized least squares (GLS) models (Aitken, 1936) with autoregressive (AR) errors (Cochrane and Orcutt, 1949) of the first order (AR(1)) were used to examine the biotic and abiotic variables influencing LE. GLS was used because eddy covariance fluxes and micrometeorological data are temporally autocorrelated, violating the independence assumption of ordinary least squares. Three models were fitted: one covering the entire year 2023 and two separating the growing season (March 15 to October 15) from the non-growing season. To control for seasonal effects, in a first step ordinary least squares (OLS) models were created for all relevant predictors (R_n, GPP, VPD, T_a and WTD) with only the months as predictors. The residuals of the OLS model are the proportions of the dependent variables that are not explained by seasonal effects, which were used as predictors for the further analysis. For all time windows (entire year, growing season, non-growing season), the data were checked for multicollinearity using the variance inflation factor (VIF), whereby all predictors had to have a VIF value of < 10 (Dormann et al., 2013). In addition, the correlation between all pairs of predictors was checked and a Pearson correlation coefficient (r) of $|r| < 0.7$ was required for all parameters (Dormann et al., 2013).

H and T_s were excluded from the models; the reason for the exclusion was a high level of multicollinearity when H was included and a strong collinearity between T_a and Ts. The detrended predictors were normalized to a mean value of 0 and a standard deviation of 1. Normalization makes it possible to compare the effect sizes.

To account for temporal autocorrelation in the residuals, a GLSAR AR(1) was used. The order of AR was chosen based on a partial autocorrelation function (PACF) plot. This GLSAR AR(1) model considers the dependency between two neighbouring points in time and assumes that the difference between the predicted and actual values (residuals) is not completely random, but is partially influenced by the previous value, which is typical for climate data. In addition, the HC3 covariance matrix correction was used to estimate the standard errors, which ensures that the standard errors are robustly estimated even in the case of heteroscedasticity. The use of HC3 is therefore a conservative estimate of the confidence intervals and p-values.

The quality of the model was assessed using the R^2 value and the Durbin-Watson statistic (DW) (Durbin and Watson, 1950, 1951, 1971). Temporal autocorrelation is assumed from a DW < 1.5 or > 2.5, whereas a value of 2 means that no temporal autocorrelation is present.

https://doi.org/10.5194/egusphere-2025-5633
Preprint. Discussion started: 5 December 2025

Working with mean daily values requires the time series to be complete, which in Eddy Covariance virtually always requires filling of gaps created during to quality checks such as u^*-filtering. Assessing drivers on gap-filled data bears the danger of circularity, since data that was filled through models is inherently dependent on the predictors used. We assessed this influence by fitting separate models using different thresholds of the maximum percentage of gap-filled values in each day (between 30% and 100%).

3 Results

3.1 Energy balance closure

The energy balance for 2023 is made up of a mean value of 26.6 W m^{-2} for LE, 10.56 W m^{-2} for H, –0.03 W m^{-2} for SHF, and 63.11 W m^{-2} for R_n. The slope of a linear regression between LE + H and R_n – SHF corresponded to 0.92 for all data (Fig. 1).

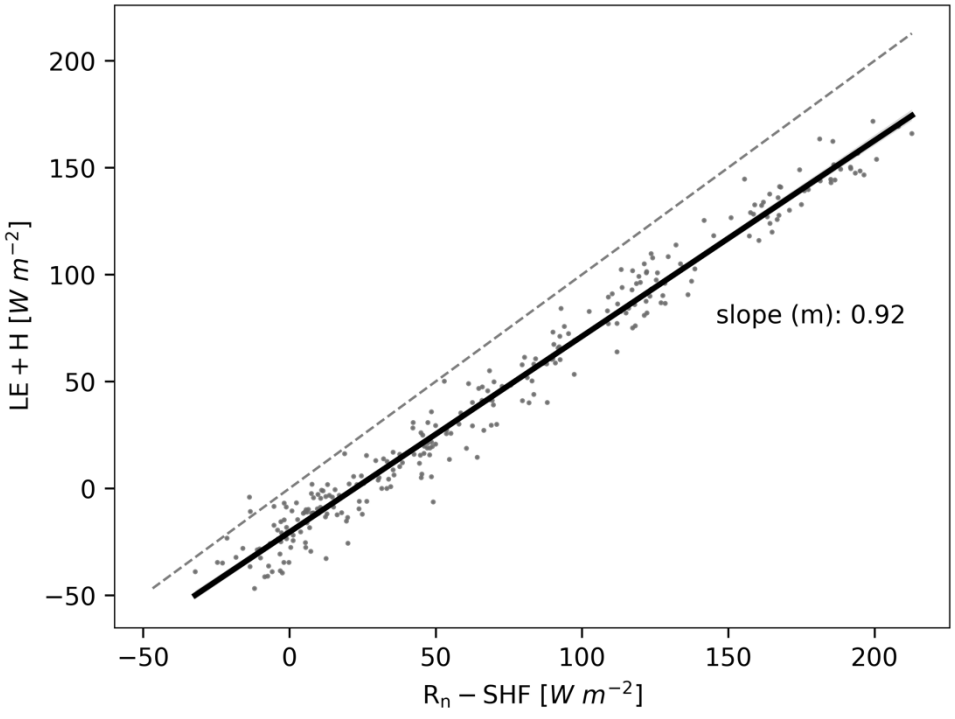

Figure 1: Test of the energy balance closure in DE-Amv during the year 2023. The x-axis shows the difference of the mean values for the net radiation (R_n) and for the soil heat flux (SHF). The y-axis shows the mean values for latent energy (LE) and sensible energy (H). Values at daily time steps are scattered against each other. A linear regression and the slope of the straight line are shown in black, while the dashed gray line shows a perfect correlation of 1.

https://doi.org/10.5194/egusphere-2025-5633
Preprint. Discussion started: 5 December 2025

3.2 Seasonal energy flux dynamics

The analysis of the monthly average daily fluctuations in the energy flux components shows clear seasonal patterns. H dominates the turbulent energy flux during most months of the first half of the year (from February to May), while LE becomes the dominant component later in the year (from July to September) (Fig. 2). This seasonal shift of the turbulent energy fluxes is reflected in B, which remains above 1 in the initial months before declining below 1 during June to October (Fig. 3).

While LE rises in the morning together with R_n, it falls in the afternoon with a delayed response to R_n. VPD and T_a also remain high during early afternoon (Fig. 4). In each month, R_n was the dominant energy component during daytime, while SHF was permanently the lowest. SHF shows a diurnal variation throughout the year, which is delayed in relation to the other energy components.

During the colder months (November to February), turbulent energy fluxes are minimal, with H frequently registering negative values and LE remaining close to zero. Consequently, B also assumes negative values with considerable fluctuations. GPP exhibits a characteristic daily pattern, rising sharply in the morning, peaking before midday, and then gradually declining. This trend mirrors the course of VPD and T_a in an axisymmetric manner. T_s follows a similar pattern to SHF, with minimum values in the morning and an increase towards the evening. Nighttime values of H drop clearly, reaching the lowest levels in winter. Conversely, LE approaches zero at night, with seasonal variations in daily maxima. All four energy flux components (R_n, SHF, H, and LE) display steady trends over the year, with smooth transitions between seasonal extremes. The daily peaks of LE and H occur after those of R_n but precede SHF maxima.

R_g peaks during June (Figure 5). Air temperature and VPD peak in July. SWC was measured at multiple locations, showing consistent trends between locations, despite local heterogeneities. The driest soil conditions are observed in late June and July, whereas the wettest period occurs between November and December, during which SWC remains relatively stable compared to other months. P exhibits seasonal variability, with the lowest amounts recorded in February and June and the highest during mid-October to December. The most intense short-term rainfall events occur primarily in the warmer months (July - September), whereas precipitation in the colder months (January to March and November to December) is more frequent but of lower intensity. WTD fluctuates throughout the year, being closer to the surface from January to mid-May before gradually declining until October. Despite data gaps in WTD, trends suggest a partial recovery to earlier levels by October.

LE reaches its highest values in July, coinciding with peak VPD and occurring one month after the R_n maximum. Although general trends are evident, deviations can be observed in all measured variables; for instance, R_g shows frequent high values in early summer (mid-May to June), which align with local maxima in T_a and VPD, coinciding with a drier period marked by low SWC and WTD. Albedo is highest during mid-to-late summer (a = 0.15) and lowest in spring and winter (a = 0.11). A qualitative visual assessment using phenocam images confirms these findings.

https://doi.org/10.5194/egusphere-2025-5633
Preprint. Discussion started: 5 December 2025

Annual precipitation reached 1023 mm y^{-1} in DE-Amv in 2023. 2023, average air temperature reached 11.7 °C in DE-Amv. Mean monthly temperature in DE-Amv was 5.3 °C in January and 20.2 °C in July. SWC ranged from 15% (June) to 56% (January, March-April, August, October-December) (Fig. 5). WTD ranged from ¬58 cm (October) to 0 cm (March). Soil temperature reached its minimum in February at 2 °C and its maximum in June and July at around 20 °C to 21 °C.

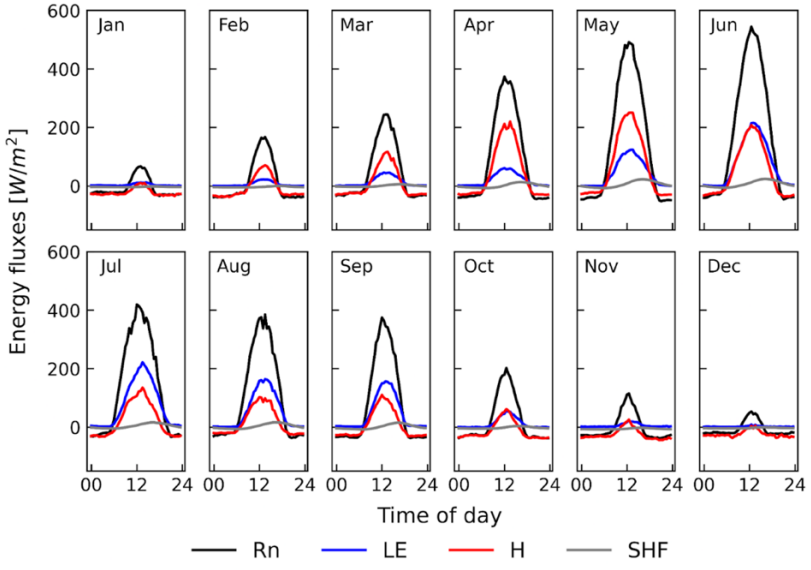

Figure 2: Monthly mean diurnal radiative and turbulent energy fluxes for the year 2023: In black the net radiation (Rn), in blue the latent energy flux (LE), in red the sensible heat flux (H) and in gray the soil heat flux (SHF). The times indicate the local time of the study site.

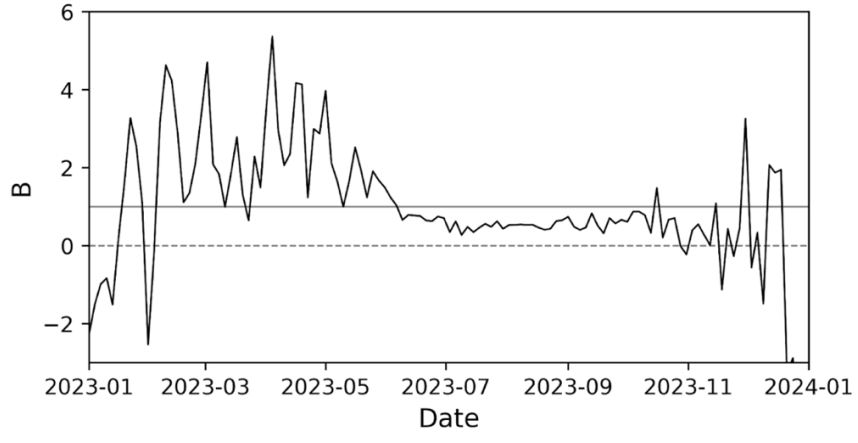

Figure 3: Bowen ratio (B) for the year 2023: The values are aggregated to three-day values. B values above 1 mean that sensible heat (H) dominates and B values below 1 (vertical solid line) indicate that latent energy (LE) assumes larger values than H.

https://doi.org/10.5194/egusphere-2025-5633
Preprint. Discussion started: 5 December 2025

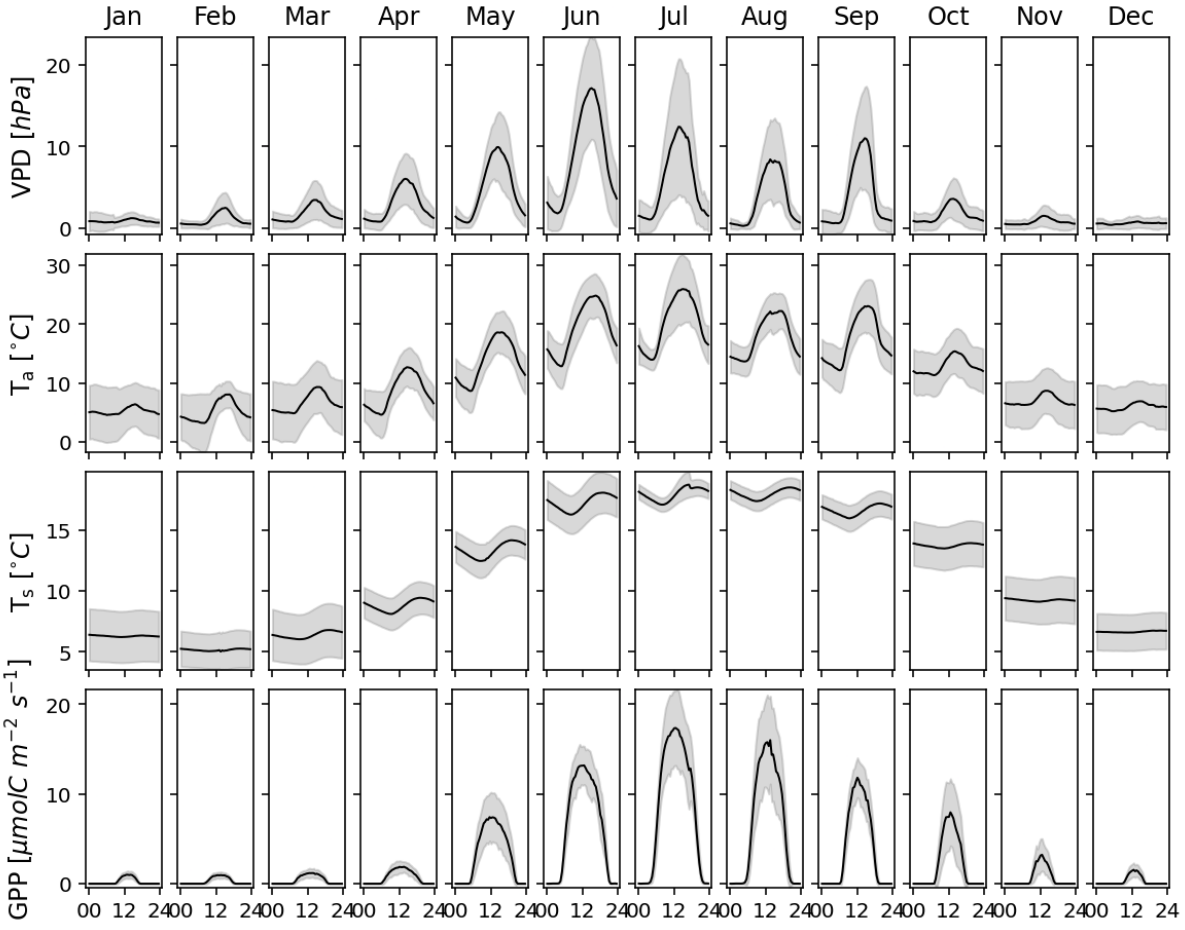

Figure 4: Diurnal patterns by month. The black line shows the mean value, while the grey area represents the standard deviation. VPD = vapor pressure deficit, T_a = air temperature, T_s = soil temperature, GPP = gross primary production.

https://doi.org/10.5194/egusphere-2025-5633
Preprint. Discussion started: 5 December 2025

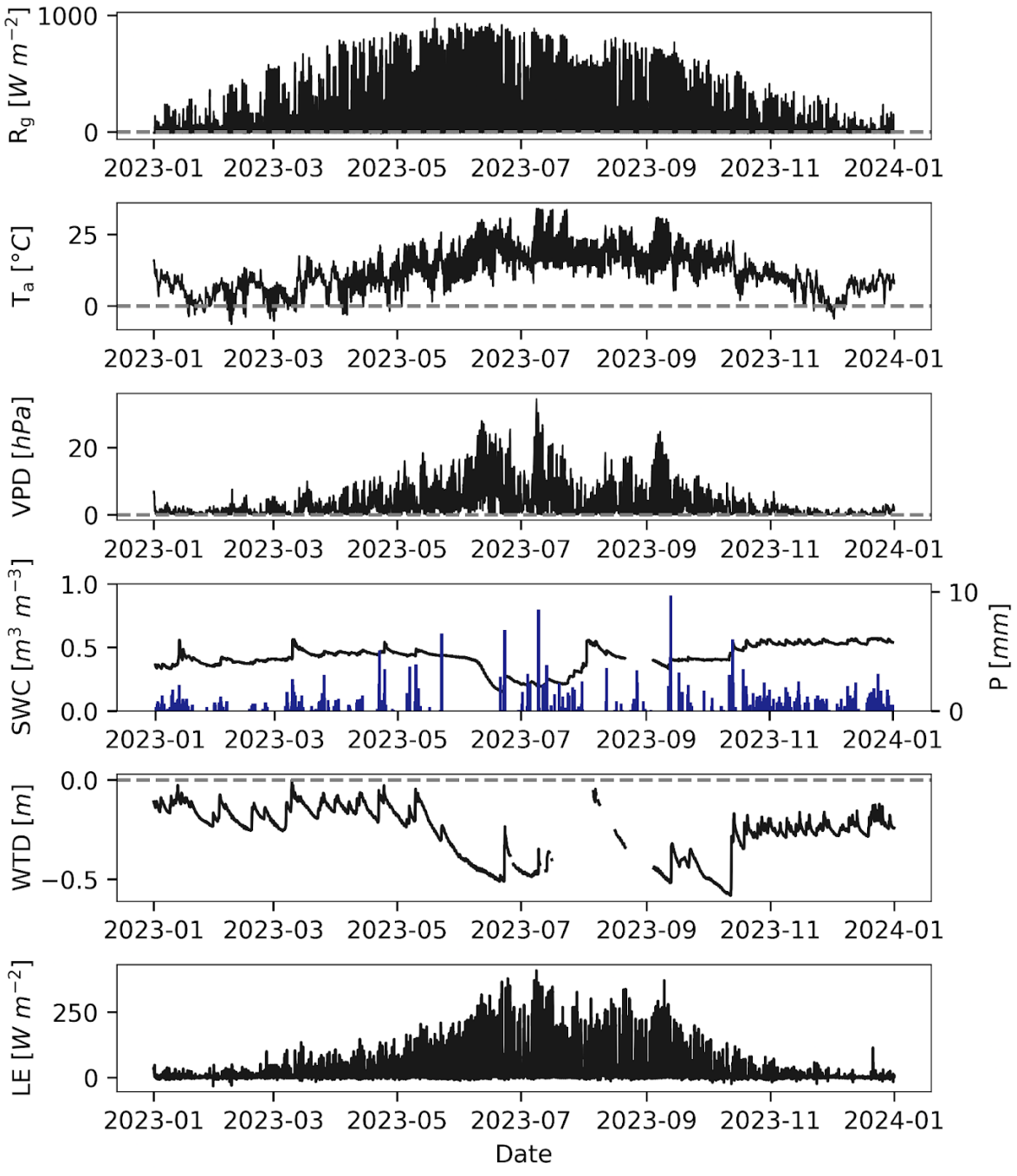

Figure 5: Global radiation (R_g), air temperature (T_a), vapor pressure deficit (VPD), soil water content (SWC) at –5 cm depth, in blue the precipitation (P), water table depth (WTD and latent energy (LE)) for the year 2023. The data is displayed in 30-minute intervals.

https://doi.org/10.5194/egusphere-2025-5633
Preprint. Discussion started: 5 December 2025

3.3 Driver analysis

The GLSAR AR(1) regression results indicate a strong model fit for 2023, during the growing and non-growing season. In all trained models VIF values were well below 10 and between the explanatory variables all R values were less than 0.7.

For the entire year 2023, the model exhibits a high goodness of fit with an R^2 of 0.777 and an adjusted R^2 of 0.773 (Table 2). The F-statistic of 117.8 ($p < 0.001$) confirms the overall significance of the model. The DB statistics of 2.041 suggests that temporal autocorrelation has been effectively corrected. During the growing season (March 15 to October 15), the model fit improves further, with an R^2 of 0.797 and an adjusted R^2 of 0.792. The F-statistic of 122.9 ($p < 0.001$) further confirms the strong explanatory power of the predictors also in the model for the growing season. The DB statistics of 2.009 remain close to the ideal value of 2, indicating near no autocorrelation. In contrast, the non-growing season shows a weaker model fit, with an R^2 of 0.671 and an adjusted R^2 of 0.659. Despite the lower explanatory power, the model remains statistically significant (F-statistic = 27.8, $p < 0.001$). The DB statistics of 2.014 suggest a good level of autocorrelation correction.

In the entire year 2023, the standardized residuals of GPP, VPD and Rn exhibit significant positive effects on LE, with coefficients of 6.8 for GPP, 6.3 for VPD, and 3.8 for R_n ($p < 0.001$) (Table 3). WTD shows no significant positive effect on LE, also, T_a has no significant effect on LE. During the growing season, all parameters considered, except WTD, show a significant influence on LE (Table 4). Net radiation influence on LE is notably stronger compared to the annual results and now has an effect size of 5.3. GPP also gains further weight during the growing season and with 8.7 has a larger effect size than VPD during this time. With a coefficient of 6.6 VPD remains an important predictor, while T_a has a medium positive effect on LE (2.5). During the non-growing season, VPD has by far the strongest effect, although at 2.9 it is weaker than in the previous two time periods (Table 5). GPP and WTD have no significant effect on LE during the non-growing season. R_n and T_a almost have no influence on LE. With –0.8 Ta's effect on LE is negative during the non-growing season. While the monthly mean value for T_a was slightly higher in January than in February and generally showed little change in the non-growing season, LE was considerably lower in January and December than in the neighbouring months.

Table 2: Metrics of GLSAR AR(1) models. Data is from 2023 and the growing season is taking place from March 15 to October 15. DB = Durbin-Watson.

Time frame	R^2	adj. R^2	F-stat.	p (F-stat.)	DB
entire year	0.777	0.773	117.8	< 0.001	2.041
growing season	0.797	0.792	122.9	< 0.001	2.009
non-growing season	0.671	0.659	27.80	< 0.001	2.014

Table 3: Results of GLSAR AR(1) model for the entire year 2023. Rn = net radiation, GPP = gross primary production, VPD = vapor pressure deficit, T_a = air temperature and WTD = water table depth.

Variable of standardized residuals	Coefficient	Standard error	t	$p > \|t\|$	[0.025	0.975]

https://doi.org/10.5194/egusphere-2025-5633
Preprint. Discussion started: 5 December 2025

R_n	3.8	1.0	3.6	< 0.001	1.7	5.8
GPP	6.8	1.0	7.0	< 0.001	4.9	8.7
VPD	6.3	1.1	5.8	< 0.001	4.1	8.4
T_a	0.6	0.6	1.0	0.333	–0.6	1.7
WTD	1.3	0.8	1.6	0.155	–0.3	2.9

Table 4: Results of GLSAR AR(1) model for the growing season (March 15 to October 15) in 2023. Rn = net radiation, GPP = gross primary production, VPD = vapor pressure deficit, T_a = air temperature and WTD = water table depth.

Variable of standardized residuals	Coefficient	Standard error	t	*p* > |t|	[0.025	0.975]
R_n	5.3	1.8	3.0	0.004	1.7	8.8
GPP	8.7	1.5	5.8	< 0.001	5.8	11.7
VPD	6.6	1.8	3.7	< 0.001	3.1	10.0
T_a	2.5	1.0	2.5	0.014	0.5	4.4
WTD	1.2	1.2	1.0	0.298	–1.103	3.6

Table 5: Results of GLSAR AR(1) model for the non-growing season (before March 15 and after October 15) 2023. Rn = net radiation, GPP = gross primary production, VPD = vapor pressure deficit, T_a = air temperature and WTD = water table depth.

Variable of standardized residuals	Coefficent	Standard error	t	*p* > |t|	[0.025	0.975]
R_n	1.0	0.3	3.5	0.001	0.4	1.5
GPP	0.5	0.2	2.5	0.014	0.1	1.0
VPD	2.9	0.4	6.8	< 0.001	2.1	3.7
T_a	–0.8	0.3	–3.0	0.004	–1.3	–0.2
WTD	0.8	0.3	2.4	0.017	0.2	1.5

3.4 Canopy conductance

The results of $g_{c,modeled}$ are daily values calculated down to mm s^{-1} and accordingly show the mean value for the individual days. $g_{c,modeled}$ shows two large gaps, which are due to a lack of data points from $g_{c,PM}$ around August and November (Fig. 6). The first gap is from July 13 to August 06 and the second gap is from October 25 to November 28. Between mid-March and

https://doi.org/10.5194/egusphere-2025-5633
Preprint. Discussion started: 5 December 2025

end of April, $g_{c,modeled}$ is around 2.5 mm s^{-1} and then rise to around 4.5 mm s^{-1} and mid-June to over 5 mm s^{-1}. There are large fluctuations and peaks of $g_{c,modeled}$ in the period from August to October compared to other times of the year. The value range over this time of large fluctuations during August to October is between 1 mm s^{-1} and 20 mm s^{-1}. In August $g_{c,modeled}$ reaches its highest values and thereafter shows a steady downward trend. $g_{c,modeled}$ values were filtered for the period from March 15 to October 15, as active vegetation can be assumed during this period. $g_{c,modeled}$ is close to 0 in the omitted periods except for three outliers in December.

$g_{c,modeled}$ was used to analyse the relationship between g_c and VPD to better understand the role of vegetation (Fig. 7). A local polynomial regression suggests a maximum $g_{c,modeled}$ (5 mm s^{-1}) at around 7 hPa VPD before gradually declining at higher VPD. Mean values for $g_{c,modeled}$ are highest around 5 hPa VPD, with substantial variability in this range, as indicated by large standard deviations (Fig. 7). Mean values of $g_{c,modeled}$ decrease after 5 hPa VPD.

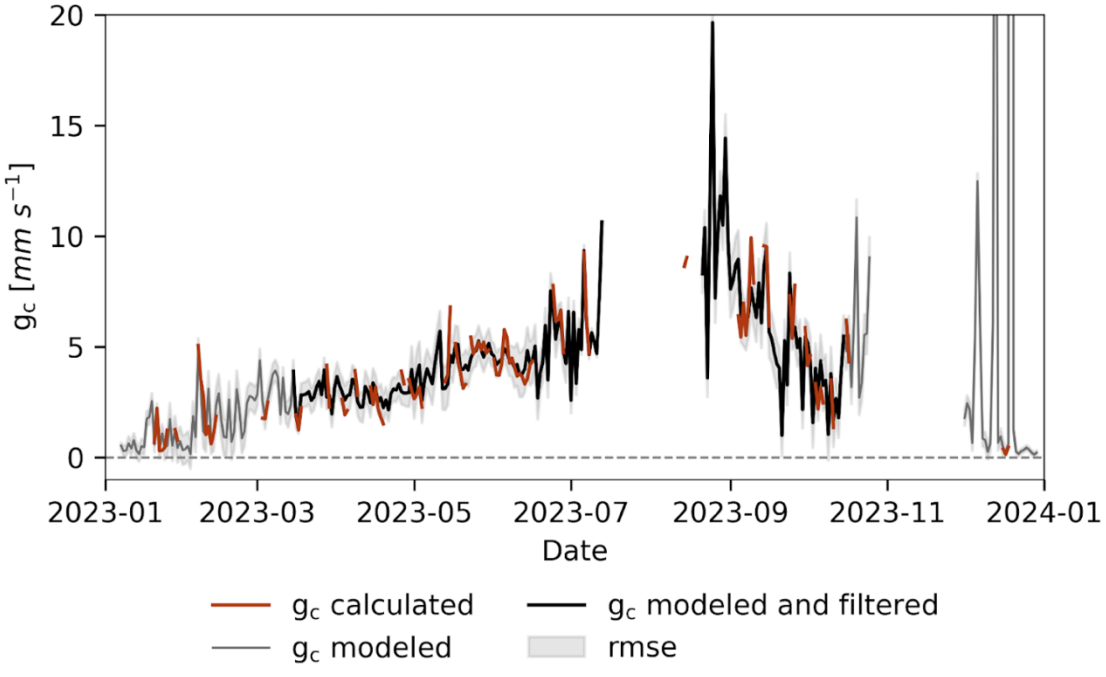

Figure 6: Canopy conductance (gc) and root mean square error (RMSE) in mm s^{-1}. In red values calculated with equation 2, in gray g_c values modeled with equation 3, in black the modeled values after filtering and the RMSE of the modeled data in light gray. The values are calculated on a daily basis.

https://doi.org/10.5194/egusphere-2025-5633
Preprint. Discussion started: 5 December 2025

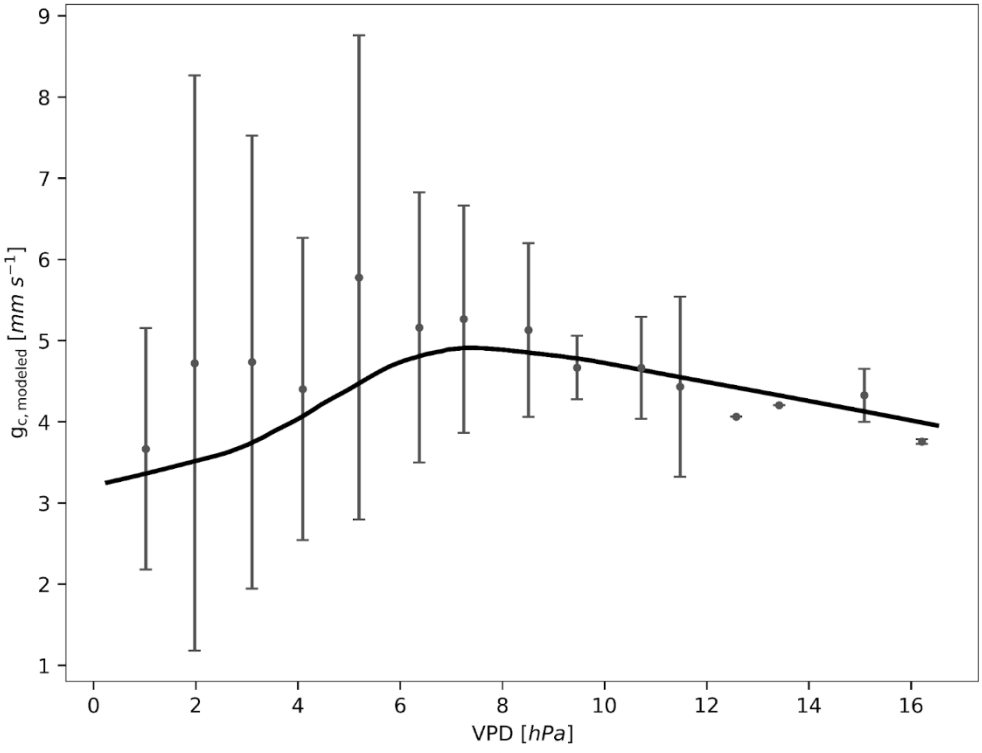

Figure 7: Relationship between modeled canopy conductance (gc,modeled) and vapor pressure deficit (VPD). The data are daily averages for gc,modeled using equation 3. In gray mean and standard deviation for individual data points, in black a local polynomial regression. The data were restricted to the period from March 15 to October 15.

3.5 Effect of gap-filled data

While we did detect an effect of the amount of gap-filled data on the model coefficients, the magnitudes of variable importances remained largely stable (Fig. A3). An in-depth discussion of the results is provided in the supplementary material (section A).

4 Discussion

This study provides the first analysis of biotic and abiotic drivers of latent heat (LE) fluxes in a peatland of the Central European lowlands. The energy balance closure was 88%, which falls within the typical range reported for the eddy covariance method (70-90%; Twine et al., 2000). In our experimental setup, part of the residual imbalance likely arose from mismatches between the source areas (footprints) of turbulent heat fluxes, net radiation, and ground heat flux. Additional sources of imbalance include low pass filtering of water vapor by the intake tube of the gas analyser, general measurement uncertainties, non-turbulent transport processes, unaccounted energy storage (e.g., in soil or biomass), and errors introduced

https://doi.org/10.5194/egusphere-2025-5633
Preprint. Discussion started: 5 December 2025

during data processing (Mauder et al., 2024). Despite these limitations, the observed closure indicates that the energy flux measurements are of sufficient quality to support robust analysis and interpretation

When comparing turbulent energy fluxes in DE-Amv with similar sites (e.g., Gerling et al., 2019), during the warm season, LE generally dominates H, regardless of the site and its local climate. Gerling et al. (2019) found Bowen ratios < 1 in a central European mountainous peatland in July and August, similar to Gunawardhana et al. (2021) in an Australian peatland and Runkle et al. (2014) in a boreal peatland, where LE was several times higher than H. In the cold season, particularly in spring, B varies across regions: Alekseychik et al. (2017) and Runkle et al. (2014) observed LE > H during all measured months in boreal peatlands, while Gunawardhana et al. (2021) found B > 1 in Australian mountains, as in DE-Amv. In fall, the mountain valley bog in Australia had B < 1, whereas in DE-Amv, LE continued to exceed H. One possible explanation is that available energy goes more into LE than into H and that this ratio only reverses when LE is limited. Mamadou et al. (2016), for example, identified water availability in the soil as the main driver for changes in the Bowen ratio, whereby they investigated two different areas (cultivated area and woodland) in Northern Benin, where a dry and a rainy season exist. However, further research is needed to be able to make reliable statements about the underlying causes of the interaction between LE and H, particularly in the considered context of peatlands.

4.1 Drivers of latent energy

The GLSAR model enabled us to disentangle the individual effects on LE, which could not be achieved using correlation coefficients alone. The strong multicollinearity observed in the correlation analysis was largely driven by the seasonal co-variation with incoming shortwave radiation (R_s). This issue was effectively mitigated through residualization, allowing for a more reliable assessment of biotic and abiotic drivers.

R_n serves as primary energy source for LE and influences it through two main mechanisms. First, it drives surface evaporation e.g., from soil. Second, it provides the energy necessary for biological activity, enabling vegetation to transpire and thereby further enhance LE. The pronounced influence of R_n on LE during the growing season likely reflects this overarching role. Outside the growing season, however, the residual aboveground vegetation in DE-Amv continues to shade the soil, limiting the direct impact of R_n on surface evaporation.

Although higher VPD physically promotes faster water evaporation, vegetation can counteract this through stomatal closure to prevent desiccation (Grossiord et al., 2020). Nevertheless, this physical relationship helps explain why VPD shows the strongest correlation with LE, particularly outside the growing season when stomatal regulation is largely absent. With global VPD expected to rise under climate change (Shekhar et al., 2024; Yuan et al., 2019), LE in DE-Amv is likely to be affected. Increases in VPD can enhance LE up to the point at which stomatal regulation limits transpiration, potentially offsetting or reversing this effect. While stomatal control has been well-documented in forest ecosystems under variable environmental conditions, our results – consistent with a limited number of studies – indicate that this mechanism also plays a significant role in peatland ecosystems. Consequently, the presence and variability of stomatal regulation across sites and vegetation types should be carefully considered in models of ecosystem energy, carbon, and water fluxes.

https://doi.org/10.5194/egusphere-2025-5633
Preprint. Discussion started: 5 December 2025

While meteorological factors such as R_n and VPD are frequently identified as the main drivers of LE (e.g., Gunawardhana et al. (2021) in a mountainous peatland), GPP is less often reported as a dominant driver. For example, Eichelmann et al. (2022) found that vegetation contributed 70 – 75% to LE in California wetlands, whereas in this study it accounted only for about one third. This discrepancy likely reflects the greater heterogeneity of vegetation compared to meteorological factors, both spatially and temporally. Furthermore, GPP is challenging to predict for the future: although it is expected to increase under climate change (Lu et al., 2024), the anticipated rise in extreme events, such as droughts, can alter the water balance and consequently GPP (Beniston et al., 2007). Therefore, further research is needed to understand how extreme events may modify the relative influence of different drivers on LE.

As the non-growing season is characterized by very low LE fluxes, very small influences such as that of T_a may not be statistically interpretable. Nevertheless, the effect size of VPD residuals is sufficiently strong (coefficient = 2.9) to assume a genuine correlation between VPD and LE during the non-growing season.

Contrary to our hypothesis, canopy conductance (g_c) peaked in summer rather than spring, suggesting a delayed response of g_c to increasing VPD. The relationship between g_c and VPD observed here does not follow the exponential pattern reported in other studies (Runkle et al., 2014; Xu et al., 2021). This deviation may result from high variability in g_c among species, leaf age, and environmental conditions (Song et al., 2022; Xu et al., 2021). For instance, Gobin et al. (2015) observed that *Calluna vulgaris* did not significantly close stomata under increasing VPD when soils were saturated, with similar results for *Molinia caerulea*, albeit at lower transpiration rates.

DE-Amv is planned for rewetting in the near future, which could alter peatland water balance, vegetation composition, canopy structure, and leaf area, thereby affecting LE. For example, if *Molinia caerulea*, which tolerates higher moisture, expands, LE could decrease (Gobin et al., 2015), while its sensitivity to VPD might remain unchanged. A more detailed evaluation of the contributions of individual functional plant groups – potentially by linking g_c with phenological patterns – will be crucial for accurately predicting future LE dynamics and understanding the role of peatland ecosystems in regulating climate through energy fluxes.

Overall, our results highlight that vegetation plays a significant and dynamic role in controlling energy fluxes in peatland ecosystems. Accurately accounting for species composition, functional traits, and stomatal regulation will be essential for predicting future latent heat dynamics and for understanding the contribution of peatlands to regional and global climate regulation.

Declaration of generative AI and AI-assisted technologies in the writing process

During the preparation of this work the author(s) used deepl.com in order to help with the translation from German into English. After using this tool/service, the author(s) reviewed and edited the content as needed and take(s) full responsibility for the content of the published article.

https://doi.org/10.5194/egusphere-2025-5633
Preprint. Discussion started: 5 December 2025

Code availability statement

Code is available upon request.

Data availability statement

Eddy covariance and micrometeorological data are available via ICOS Carbon Portal under doi.org/10.18160/S6HM-CP8Q.

Declaration of competing interest

The authors declare no conflict of interest.

Author contribution

VF: formal analysis, methodology, software, visualization, writing (original draft preparation), writing (review and editing). NB: data curation, formal analysis, methodology, supervision, validation, writing (review and editing). MG: conceptualization, funding acquisition, methodology, project administration, resources, supervision, validation, writing (review and editing).

References

Aitken, A.C., 1936. IV.—On Least Squares and Linear Combination of Observations. Proc. R. Soc. Edinb. 55, 42–48.

Alekseychik, P., Mammarella, I., Karpov, D., Dengel, S., Terentieva, I., Sabrekov, A., Glagolev, M., Lapshina, E., 2017. Net ecosystem exchange and energy fluxes measured with the eddy covariance technique in a western Siberian bog. Atmos. Chem. Phys. 17 (15), 9333–9345.

Beniston, M., Stephenson, D.B., Christensen, O.B., Ferro, C.A.T., Frei, C., Goyette, S., Halsnaes, K., Holt, T., Jylhä, K., Koffi, B., Palutikof, J., Schöll, R., Semmler, T., Woth, K., 2007. Future extreme events in European climate: an exploration of regional climate model projections. Climatic Change 81 (S1), 71–95.

Chen, T., Guestrin, C., 2016. XGBoost. Machinery, New York, USA, 785–794. doi:10.1145/2939672.2939785.

Cochrane, D., Orcutt, G.H., 1949. Application of Least Squares Regression to Relationships Containing Auto-Correlated Error Terms. Journal of the American Statistical Association 44 (245), 32–61.

Dingman, S.L., 2015. Physical hydrology, Third edition ed. Waveland Press Inc, Long Grove, Illinois, 643 pp.

Directorate-General for Environment, 2024. Natura 2000. https://environment.ec.europa.eu/topics/nature-and-biodiversity/natura-2000_en.

https://doi.org/10.5194/egusphere-2025-5633
Preprint. Discussion started: 5 December 2025

Dormann, C.F., Elith, J., Bacher, S., Buchmann, C., Carl, G., Carré, G., Marquéz, J.R.G., Gruber, B., Lafourcade, B., Leitão, P.J., Münkemüller, T., McClean, C., Osborne, P.E., Reineking, B., Schröder, B., Skidmore, A.K., Zurell, D., Lautenbach, S., 2013. Collinearity: a review of methods to deal with it and a simulation study evaluating their performance. Ecography 36 (1), 27–46.

Durbin, J., Watson, G.S., 1950. Testing for Serial Correlation in Least Squares Regression: I. Biometrika 37 (3/4), 409.

Durbin, J., Watson, G.S., 1951. Testing for Serial Correlation in Least Squares Regression. II. Biometrika 38 (1-2), 159–178.

Durbin, J., Watson, G.S., 1971. Testing for Serial Correlation in Least Squares Regression. III. Biometrika 58 (1), 1.

DWD, 2022. Climate Data Center. https://cdc.dwd.de/portal/202209231028/view1. Accessed 12 April 2024.

Eichelmann, E., Mantoani, M.C., Chamberlain, S.D., Hemes, K.S., Oikawa, P.Y., Szutu, D., Valach, A., Verfaillie, J., Baldocchi, D.D., 2022. A novel approach to partitioning evapotranspiration into evaporation and transpiration in flooded ecosystems. Global change biology 28 (3), 990–1007.

Europäische Union, 2021. Standard-Datenbogen: DE3807301, in: Landesamt für Natur, Umwelt und Verbraucherschutz Nordrhein-Westfalen (Ed.), Natura 2000-Gebiete in Nordrhein-Westfalen - Fachinformation - Listen der Natura 2000-Gebiete.

Fay, E., Lavoie, C., 2009. The impact of birch seedlings on evapotranspiration from a mined peatland: an experimental study in southern Quebec, Canada. Mires and Peat 5.

Gerling, L., Weber, T.K., Reineke, D., Durner, W., Martin, S., Weber, S., 2019. Eddy covariance based surface-atmosphere exchange and crop coefficient determination in a mountainous peatland. Ecohydrology 12 (1).

Gobin, R., Korboulewsky, N., Dumas, Y., Balandier, P., 2015. Transpiration of four common understorey plant species according to drought intensity in temperate forests. Annals of Forest Science 72 (8), 1053–1064.

Grossiord, C., Buckley, T.N., Cernusak, L.A., Novick, K.A., Poulter, B., Siegwolf, R.T.W., Sperry, J.S., McDowell, N.G., 2020. Plant responses to rising vapor pressure deficit. The New phytologist 226 (6), 1550–1566.

Gunawardhana, M., Silvester, E., Jones, O.A., Grover, S., 2021. Evapotranspiration and biogeochemical regulation in a mountain peatland: insights from eddy covariance and ionic balance measurements. Journal of Hydrology: Regional Studies 36, 100851.

Harris, C.R., Millman, K.J., van der Walt, S.J., Gommers, R., Virtanen, P., Cournapeau, D., Wieser, E., Taylor, J., Berg, S., Smith, N.J., et al., 2020. Array programming with NumPy. Nature 585 (7825), 357–362.

Heijmans, M.M.P.D., van der Knaap, Y.A.M., Holmgren, M., Limpens, J., 2013. Persistent versus transient tree encroachment of temperate peat bogs: effects of climate warming and drought events. Global change biology 19 (7), 2240–2250.

Humphreys, E.R., Lafleur, P.M., Flanagan, L.B., Hedstrom, N., Syed, K.H., Glenn, A.J., Granger, R., 2006. Summer carbon dioxide and water vapor fluxes across a range of northern peatlands. J. Geophys. Res. 111 (G4).

Hunter, J.D., 2007. Matplotlib: A 2D Graphics Environment. Comput. Sci. Eng. 9 (3), 90–95.

https://doi.org/10.5194/egusphere-2025-5633
Preprint. Discussion started: 5 December 2025

Karimi, S., Maher Hasselquist, E., Salimi, S., Järveoja, J., Laudon, H., 2024. Rewetting impact on the hydrological function of a drained peatland in the boreal landscape. Journal of Hydrology 641, 131729.

Kettridge, N., Waddington, J.M., 2014. Towards quantifying the negative feedback regulation of peatland evaporation to drought. Hydrological Processes 28 (11), 3728–3740.

Kottek, M., Grieser, J., Beck, C., Rudolf, B., Rubel, F., 2006. World Map of the Köppen-Geiger climate classification updated. metz 15 (3), 259–263.

Lafleur, P.M., Hember, R.A., Admiral, S.W., Roulet, N.T., 2005. Annual and seasonal variability in evapotranspiration and water table at a shrub-covered bog in southern Ontario, Canada. Hydrological Processes 19 (18), 3533–3550.

Liu, H., Rezanezhad, F., Lennartz, B., 2022. Impact of land management on available water capacity and water storage of peatlands. Geoderma 406, 115521.

Lu, Q., Liu, H., Wei, L., Zhong, Y., Zhou, Z., 2024. Global prediction of gross primary productivity under future climate change. The Science of the total environment 912, 169239.

Mamadou, O., Galle, S., Cohard, J.-M., Peugeot, C., Kounouhewa, B., Biron, R., Hector, B., Zannou, A.B., 2016. Dynamics of water vapor and energy exchanges above two contrasting Sudanian climate ecosystems in Northern Benin (West Africa). JGR Atmospheres 121 (19).

Mauder, M., Jung, M., Stoy, P., Nelson, J., Wanner, L., 2024. Energy balance closure at FLUXNET sites revisited. Agricultural and Forest Meteorology 358, 110235.

Moore, P.A., Pypker, T.G., Waddington, J.M., 2013. Effect of long-term water table manipulation on peatland evapotranspiration. Agricultural and Forest Meteorology 178-179, 106–119.

Moré, J.J., 1977. The Levenberg-Marquardt algorithm: Implementation and theory.

Nijp, J.J., Metselaar, K., Limpens, J., Teutschbein, C., Peichl, M., Nilsson, M.B., Berendse, F., van der Zee, S.E.A.T.M., 2017. Including hydrological self-regulating processes in peatland models: Effects on peatmoss drought projections. The Science of the total environment 580, 1389–1400.

Pastorello, G., Trotta, C., Canfora, E., Chu, H., Christianson, D., Cheah, Y.-W., Poindexter, C., Chen, J., Elbashandy, A., Humphrey, M., et al., 2020. The FLUXNET2015 dataset and the ONEFlux processing pipeline for eddy covariance data. Scientific data 7 (1), 225.

Pedregosa, F., Varoquaux, G., Gramfort, A., Michel, V., Thirion, B., Grisel, O., Blondel, M., Prettenhofer, P., Weiss, R., Dubourg, V., VanderPlas, J., Passos, A., Cournapeau, D., Brucher, M., Perrot, M., Duchesnay, É., 2011. Scikit-learn: Machine Learning in Python. Journal of Machine Learning Research (12), 2825–2830.

Plotly Technologies Inc., 2015. Collaborative data science. https://plot.ly.

Runkle, B.R.K., Wille, C., Gažovič, M., Wilmking, M., Kutzbach, L., 2014. The surface energy balance and its drivers in a boreal peatland fen of northwestern Russia. Journal of Hydrology 511, 359–373.

Seabold, S., Perktold, J. Statsmodels: Econometric and Statistical Modeling with Python, 92–96.

https://doi.org/10.5194/egusphere-2025-5633
Preprint. Discussion started: 5 December 2025

Shekhar, A., Buchmann, N., Humphrey, V., Gharun, M., 2024. More than three-fold increase in compound soil and air dryness across Europe by the end of 21st century. Weather and Climate Extremes 44, 100666.

Song, L., Zhu, J., Li, X., Wang, K., Wang, G., Sun, H., 2022. Transpiration of Pinus sylvestris var. mongolica trees at different positions of sand dunes in a semiarid sandy region of Northeast China. Trees 36 (2), 749–762.

Sonnentag, O., van der Kamp, G., Barr, A.G., Chen, J.M., 2010. On the relationship between water table depth and water vapor and carbon dioxide fluxes in a minerotrophic fen. Global change biology 16 (6), 1762–1776.

The pandas development team, 2025. pandas-dev/pandas: Pandas.

Truong, C., Oudre, L., Vayatis, N., 2020. Selective review of offline change point detection methods. Signal Processing 167, 107299.

Twine, T.E., Kustas, W.P., Norman, J.M., Cook, D.R., Houser, P.R., Meyers, T.P., Prueger, J.H., Starks, P.J., Wesely, M.L., 2000. Correcting eddy-covariance flux underestimates over a grassland. Agricultural and Forest Meteorology 103 (3), 279–300.

Utikal, J., Rückriem, C., 2019. Maßnahmenkonzept: Natura 2000 Amtsvenn und Hündfelder Moor DE-3807-301, in: Landesamt für Natur, Umwelt und Verbraucherschutz Nordrhein-Westfalen (Ed.), Natura 2000-Gebiete in Nordrhein-Westfalen - Fachinformation - Listen der Natura 2000-Gebiete.

van Rossum, G., Drake, F.L., 2009. Python 3 reference manual. CreateSpace.

Virtanen, P., Gommers, R., Oliphant, T.E., Haberland, M., Reddy, T., Cournapeau, D., Burovski, E., Peterson, P., Weckesser, W., Bright, J., et al., 2020. SciPy 1.0: fundamental algorithms for scientific computing in Python. Nature methods 17 (3), 261–272.

Wutzler, T., Lucas-Moffat, A., Migliavacca, M., Knauer, J., Sickel, K., Šigut, L., Menzer, O., Reichstein, M., 2018. Basic and extensible post-processing of eddy covariance flux data with REddyProc. Biogeosciences 15 (16), 5015–5030.

Xu, J., Wu, B., Ryu, D., Yan, N., Zhu, W., Ma, Z., 2021. Quantifying the contribution of biophysical and environmental factors in uncertainty of modeling canopy conductance. Journal of Hydrology 592, 125612.

Yu, Z.C., 2012. Northern peatland carbon stocks and dynamics: a review. Biogeosciences 9 (10), 4071–4085.

Yuan, W., Zheng, Y., Piao, S., Ciais, P., Lombardozzi, D., Wang, Y., Ryu, Y., Chen, G., Dong, W., Hu, Z., et al., 2019. Increased atmospheric vapor pressure deficit reduces global vegetation growth. Science advances 5 (8), eaax1396.